Evaluating the influence of manufacturing tolerances in permanent magnet synchronous machines

I. Coenen, T. Herold, C. Piantsop Mbo'o, and K. Hameyer

Institute of Electrical Machines, RWTH Aachen University, Schinkelstrasse 4, D-52056 Aachen, Germany
E-mail: isabel.coenen@iem.rwth-aachen.de

***Abstract*—Manufacturing tolerances can result in an unwanted behavior of electrical machines. Undesired parasitic effects such as torque ripples may be increased. A quality control of machines subsequent to manufacturing is therefore required in order to test whether the machines comply with its specifications. This is useful to ensure a high reliability of the manufactured machines. This paper describes the consideration of rotor tolerances due to non-ideal manufacturing processes. The idea is to estimate the influence of the manufacturing tolerances for realization of a reliable quality control. To study various fault scenarios numerical field simulations are employed which are parameterized by measurements.**

***Index Terms*—electrical machines, Finite Element Analysis (FEA), manufacturing tolerances, quality control.**

I. Introduction

The reliability of electrical drives [1] is an important aspect to ensure a high availability. In industrial applications, permanent magnet excited synchronous machines (PMSM) are widely employed as they offer advantages in efficiency and power density. However, especially the rotor of PMSMs is susceptible to tolerances caused during mass production. Variations from the ideal machine influence its operational behavior [2]. Therefore, it is important to verify the machine's quality prior to its installation.

Reliable and widely used diagnostic methods are vibration and current monitoring [3]. In this study, electrical quantities are focused because this offers the advantage that no additional sensors need to be installed [4].

A. Proposed monitoring setup

The most often proposed end-of-line test is back-EMF monitoring [5], [6]. Fig. 1 shows a possible setup for its realization. Here, the motor under test is driven under open-circuit conditions. For attenuation of the drive's influence, a flywheel is employed between drive and motor under test.

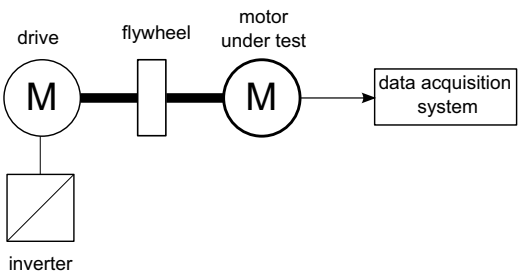

Fig. 1. Back-EMF monitoring setup.

This approach presents a non invasive monitoring method being benefical for diagnosis. However, such a setup is very expensive. It is cost-expensive because a drive is required and a certain device is needed to damp possible influences of the drive. Above all, it is time-expensive due to the fact that the motor under test is mechanically coupled to the drive. This is not an efficient solution when a large number of machines needs to be tested during mass production.

In this study, an additional approach is investigated where the current is being monitored. The corresponding setup is shown in Fig. 2. Here, a start-up of the motor up to a certain speed is performed in such a way that the current is measured at various speeds. The benefit of this method is its time- and cost-saving setup. When compared to the back-EMF setup, less hardware is needed. No mechanical coupling to a drive is required, simply the motor is connected to the inverter.

However, for evaluating the current, it needs to be considered that the current is a controlled quantity. Impacts caused by the control system or the inverter supply might lead to misinterpretation of the results.

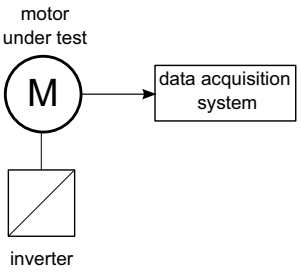

Fig. 2. Current monitoring setup.

In the following, the back-EMF and current characteristic of a PMSM is determined. In order to study various fault scenarios, numerical field calculation is employed considering tolerance affected rotor components. The aim is to evaluate the influence of such tolerances to be able to determine distinguishing characteristics. This information

can be helpful to develop an appropriate end-of-line test and to reveal which of the proposed setups is most qualified.

II. Motor under study

The machine studied within this work is a three-phase permanent magnet synchronous machine with tooth-coil winding system. It presents six stator slots and four pole pairs p. The eight magnets of the rotor are arranged in a spoke configuration.

III. Influence of rotor tolerances

During the manufacturing process material dependant failures, geometrical or shape deviations may occur. Such tolerances influence the machine's behavior. For instance, increased torque ripples are caused [7].

The considered tolerances within this paper concern the magnet's material and its dimensions. The magnetization faults are illustrated Fig. 3. Possible deviations affect the magnitude of the remanence flux density B_R and the angle β of the magnetization direction. Further

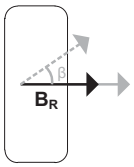

Fig. 3. Magnetization faults.

examples of rotor tolerances, not considered within this study, would be a displacement of the magnet and rotor eccentricity.

A. Theoretical analysis

Within this study, the influence of rotor tolerances onto electrical signals is focused. According to [5], for non-ideal rotor components new harmonic orders n_{rf} are expected to appear in the back-EMF spectrum which are a function of the pole pair number p:

$$n_{rf} = 1 \pm \frac{k}{p} \text{ with } k \in \mathbb{N}. \tag{1}$$

In the following, this relation shall be approved and specialized for the certain machine investigated.

The back-EMF V_i is the induced voltage at no load condition (open circuit). For a coil with w numbers of turns V_i is defined as follows:

$$V_i = -w\frac{d\phi}{dt} = -w\frac{d}{dt}(\iint \vec{B}d\vec{A}). \tag{2}$$

Applied to a machine's winding, it means that the back-EMF in one coil of the winding is determined by the air gap flux density B. Therefore the back-EMF presents the same harmonic orders which appear in the spectrum of the flux density. The latter will be considered for an order analysis.

The magnetic flux density at the air gap of the machine is a rotating wave which is a function of relative position at the air gap α and time t [8]. It is given as the product of the magnetomotive force Θ (MMF) and the air gap permeance Λ:

$$B(\alpha, t) = \Theta(\alpha, t) \cdot \Lambda(\alpha, t). \tag{3}$$

The functions of permeance, magnetomotive force and flux density can generally be represented by a series of space and time harmonics [9]:

$$\Lambda(\alpha, t) = \sum_{y_l, z_l} \Lambda_{y_l, z_l} \cdot cos(y_l \cdot \alpha - z_l \cdot t), \tag{4}$$

$$\Theta(\alpha, t) = \sum_{y_t, z_t} \Theta_{y_t, z_t} \cdot cos(y_t \cdot \alpha - z_t \cdot t), \tag{5}$$

$$B(\alpha, t) = \sum_{y_b, z_b} B_{y_b, z_b} \cdot cos(y_b \cdot \alpha - z_b \cdot t). \tag{6}$$

At this, ω_1 is the supplying angular frequency. For reasons of illustration the phase angle is neglected.

For derivation of the new harmonic orders caused by non-ideal rotor components only the rotor fundamental component of the MMF is considered, meaning $y_t = p$ and $z_t = \omega_1$. Furthermore, a constant air gap width is considered, meaning $y_l = 0$ and $z_l = 0$. For the faultless case, this implies:

$$B_p(\alpha, t) = B_{p,\omega_1} \cdot cos(p \cdot \alpha - \omega_1 \cdot t). \tag{7}$$

The above mentioned rotor tolerances lead to an asymmetrical distribution of the air gap field. With the described approach, this means a modulation of the MMF caused by the rotor magnets. New space and time harmonics k with $k \in \mathbb{N}$ appear resulting in the following expression for the flux density considering non-ideal rotor components:

$$B_{rf}(\alpha, t) = \sum_k B_k \cdot cos((p \pm k) \cdot \alpha - (\omega_1 \pm k\omega_m) \cdot t). \tag{8}$$

Here, ω_m is the rotational speed with $\omega_m = \frac{\omega_1}{p}$. Hence, B_{rf} can be expressed as follows:

$$B_{rf}(\alpha, t) = \sum_k B_k \cdot cos((p \pm k) \cdot \alpha - (1 \pm \frac{k}{p}) \cdot \omega_1 t). \tag{9}$$

This expression indicates the new harmonic orders appearing in the spectrum of the flux density and equally in the back-EMF spectrum due to deviations at the machine's rotor as predicted in expression (1). However, it is only valid considering one single coil [10]. Derivating the harmonics for one phase, the coil configuration needs to be considered. One phase of the investigated machine contains two coils which are displaced by $180°$.

According to (9) the back-EMF of the first coil in one phase assuming faulty rotor components can be

determined as follows:

$$V_{irf1}(\alpha,t) = \sum_k V_{ik} \cdot cos((p \pm k) \cdot 0^\circ - (1 \pm \frac{k}{p}) \cdot \omega_1 t). \quad (10)$$

Similarly, the back-EMF of the second coil in the same phase is:

$$V_{irf2}(\alpha,t) = \sum_k V_{ik} \cdot cos((p \pm k) \cdot 180^\circ - (1 \pm \frac{k}{p}) \cdot \omega_1 t). \quad (11)$$

The resulting back-EMF V_{irfph} for one phase can be determined by the superposition of the two coils:

$$V_{irfph} = V_{irf1} + V_{irf2} = \sum_k V_{ik} cos((1 \pm \frac{k}{p})\omega_1 t) \cdot [1 + cos((p \pm k) \cdot 180^\circ)]. \quad (12)$$

For odd numbers $(p \pm k)$, (12) is equal to zero. With $p = 4$ it is obvious that only even numbers of k appear in the back-EMF spectrum.

Finally, (1) can be specialized for the analyzed machine, indicating the new harmonic orders appearing in the spectrum of back-EMF in case of non-ideal rotor components:

$$n'_{rf} = 1 \pm \frac{2k'}{p} \text{ with } k' \in \mathbb{N}. \quad (13)$$

For the faultless case where the air gap field is symmetrical, the appearing orders are determined by the winding arrangement [5]. Considering a three phase winding, these harmonic orders are:

$$n = 6m \pm 1 \text{ with } m \in \mathbb{N}. \quad (14)$$

The mentioned new harmonic orders caused by faults appear in addition to (14).

For the current, the harmonic orders can be derived analogously. Ampere's law reveals the general relation between electrical current I and magnetic flux density B:

$$\mu_0 \cdot I = \oint_S \vec{B} d\vec{s}. \quad (15)$$

In practice, the current may additionally be affected by the control system and by the inverter supply. These impacts need to be considered in order to avoid wrong interpretation of the measured signals.

IV. Methodology

To determine the influence of the rotor tolerances onto the back-EMF and current characteristic, numerical field simulations are used. Reliable analysis requires a sufficiently large number of experiments which means less effort performing with simulation instead of measurements. In addition, the interpretation of measurement results is difficult within this context, as for a certain prototype the real existing deviations are unknown. The intentional construction of tolerances is very difficult to realize.

A. Finite Element Analysis

To calculate the back-EMF, a two-dimensional time-stepping Finite Element Analysis (FEA) is applied. No-load operation at a speed of 3000 rpm is assumed and the voltage is calculated by use of the time derivative of the magnetic flux, as in equation (2).

For analysis, a discrete Fourier transform (DFT) is performed which yields the spectrum of back-EMF as shown in Fig. 4. For the ideal faultless case with symmetrical air gap field, harmonic orders appear according to (14).

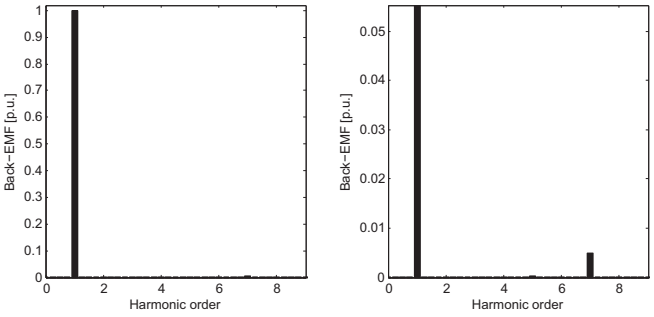

Fig. 4. Back-EMF spectrum assuming faultless case.

1) Parameterization by statistical measurements: For parameterization of the FEA model, a statistical verification is performed. The back-EMF is measured for ten prototypes of the machine. The resulting first order is evaluated in form of a histogram shown in Fig. 5. Based on this results, the magnets material properties (B_R) within the model are adjusted in order that simulated value of first order and mean value of measured first order agree.

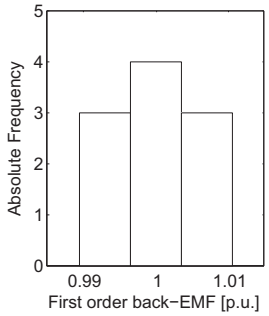

Fig. 5. Measured Back-EMF histogram.

B. Extended d-q model

A d-q model is a common way to describe the PMSM's dynamical behavior considering the control system. Here, the application of such a model is studied to calculate the current. Since the common d-q model only takes the fundamental wave into account, it is not able to consider non-ideal behavior such as local defects studied within this work. Hence, an extended d-q model [11] is applied

to calculate the current. Here, FEA is used to extract additional elements to extend the common d-q equations.

In the following, a start-up of the machine from zero to 3000 rpm is simulated and the stator current is analyzed by use of a short-time Fourier transform (STFT). This yields the spectrum including the frequency distribution over time of the non-stationary current signal. Fig. 6 shows the result for the faultless case. The value of current is represented by a color range, where light colors mean a high and dark colors a low value. It can be seen that the harmonic orders are the same as for the back-EMF.

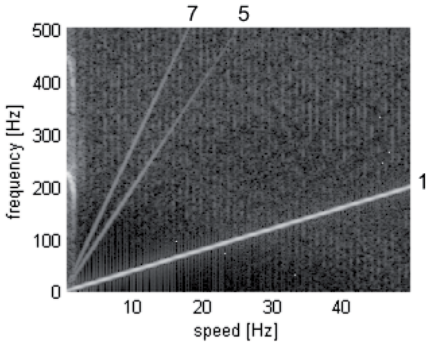

Fig. 6. Current spectrum assuming faultless case.

Here, sine-wave excitation is assumed. With the presented model it is also possible to simulate inverter operation. However, modeling the inverter leads to a computationally expensive model. Fig. 7 shows the result for the faultless case assuming inverter supply. Due to the high intensity of computation it is illustrated with lower resolution. Besides the main harmonic orders some new orders appear. However, these do not interfere with the orders which are expected to appear correspending to (13) due to tolerances. Therefore, inverter supply is not considered within this study because of the computational costs.

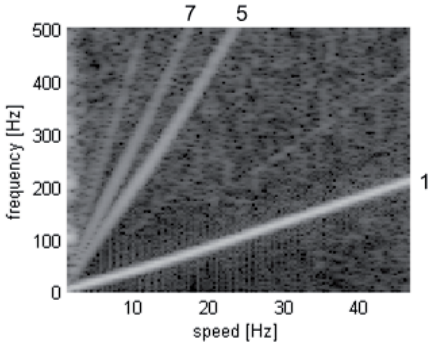

Fig. 7. Current spectrum assuming faultless case and inverter supply.

V. Simulation results

To develop a reliable end-of-line check, the most common and important fault modes should be captured. In the following, different approaches are applied to simulate various fault scenarios. The choice of the corresponding approach depends on the particular fault, the prior knowledge of the fault and the available data.

A. Worst-case analysis

For PMSMs cogging torque is an undesired effect as it leads to rotational oscillations of the drive train. Cogging torque is strongly influence by deviations caused by the manufacturing process [2],[7]. However, measuring cogging torque is very time- and cost-expensive [12] and therefore no appropiate method for an end-of-line control. In the following it shall be studied how back-EMF and current are influenced at a faulty machine presenting a high value of cogging torque due to magnetization faults.

Considering a deviation in the magnitude of the magnets' remanence flux density B_R, the amount of variation of cogging torque is depending on which and how many permanent magnets are affected. In [13] Design-of-Experiments is applied to find out the worst-case configuration of magnetization faults concerning cogging torque. Applied to the studied machine, the configuration shown in Fig. 8 presents the highest value of peak-to-peak cogging torque. Thereby, the filled magnets represent the ones that are defective. Considering a deviation at B_R of -10%, the value of cogging torque is about seven-times higher compared to the reference value of the ideal machine.

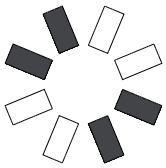

Fig. 8. Worst-case configuration of magnetization faults.

Fig. 9 and Fig. 10 show the results for back-EMF and current in case of the described worst-case magnetization fault.

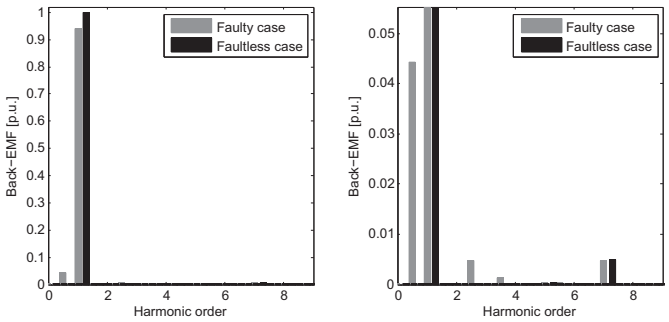

Fig. 9. Back-EMF spectrum assuming worst-case magnetization fault.

The spectra show new harmonic orders, especially $n'_{rf} = 0.5$ and $n'_{rf} = 2.5$ are apparent according to (1). Compared to the faultless case the first harmonic order is reduced.

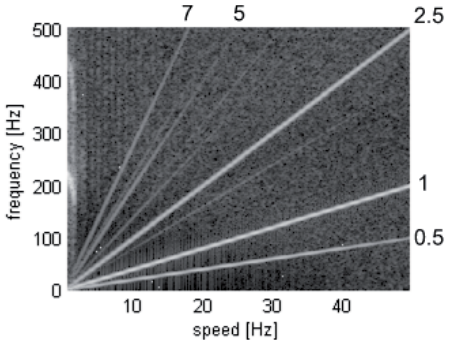

Fig. 10. Current spectrum assuming worst-case magnetization fault.

B. Sample cases

For the studied machine the height of the magnet can vary between 97% and 100% of its desired value and the width can vary by $\pm 1.5\%$. The dimensions of some sample magnets have been measured which are used as input data for this approach. None of the measured dimensions exceed the allowed tolerance range. Five cases are created where every magnet is subjected to the given tolerances. Fig. 11 and Fig. 12 exemplarily show the back-EMF and current spectrum of one faulty case. The first harmonic order is reduced compared to the faultless case and the new ordinal numbers appear corresponding to (13).

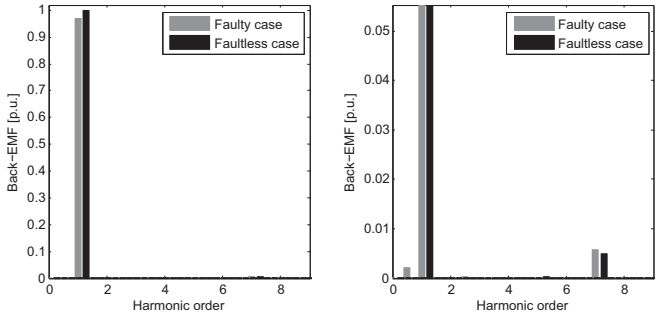

Fig. 11. Back-EMF spectrum assuming faulty magnet dimensions.

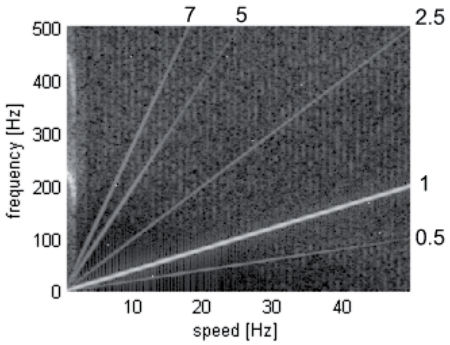

Fig. 12. Current spectrum assuming faulty magnet dimensions.

When compared to the results from the worst-case magnetization fault studied in V-A, one can see that the influence of deviations at the magnets' dimensions within the allowed tolerance range is not significant. The spectra show the same specific charateristics but less amounts. For all five studied cases the simulated spectra do not differ considerably from the faultless case.

C. Stochastic analysis

In [14] the influence of varying qualities of the permanent magnet has been investigated applying a stochastic analysis. This is applied here to compare the influences of deviations in the magnetization magnitude and magnetization direction. Overall, 60 failure configurations are studied. For 20 cases the remanence flux density B_R is assumed to be Gaussian distributed with a standard deviation of 3σ equal to 10% of the nominal value. For 20 other cases the magnetization direction is also assumed to be normally distributed with a standard deviation of $5°$. The other 20 cases present both kind of deviations. Applying FEA, cogging torque and back-EMF are calculated and evaluated employing histograms.

The distribution of the first harmonic order of the back-EMF is shown in Fig. 13. It shows the range in which the back-EMF is influenced because of the different magnetization deviations.

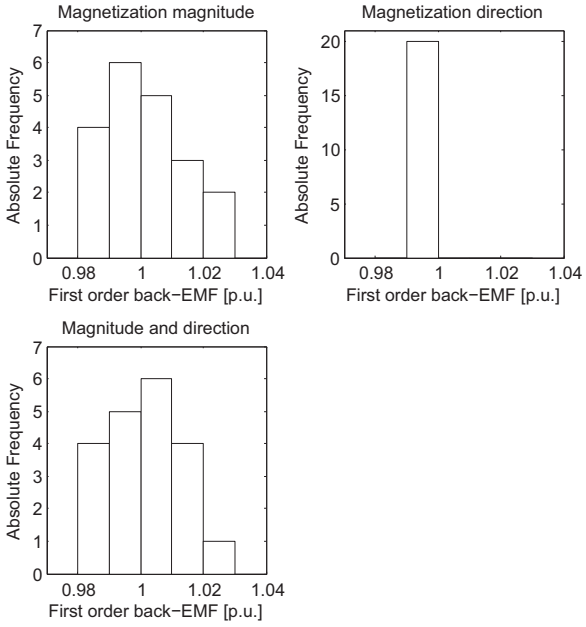

Fig. 13. Back-EMF histogram considering magnetization faults.

It can be seen that the influence of the deviations concerning the magnetization direction is very small. The magnitude fault is prevailing. This is to be expected for the studied machine as it presents interior magnets.

The same analysis is performed for the peak-to-peak cogging torque, which is presented in Fig. 14. Again it can be concluded that the influence of magnetization direction is small when compared to the deviation in magnitude as the corresponding distribution shows.

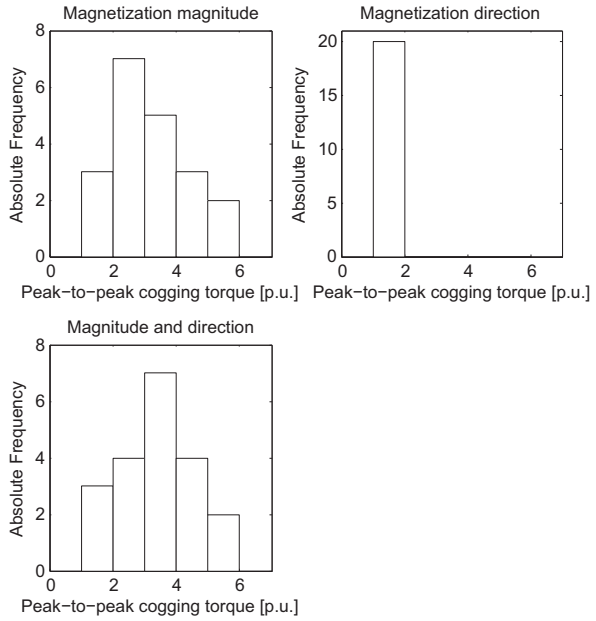

Fig. 14. Cogging torque histogram considering magnetization faults.

Generally, magnetization faults influence cogging torque and back-EMF characteristic simultaneously [15]. For both quantities new harmonic orders arise depending on the caused asymmetry in the air gap field. Based on the presented studies, it becomes apparant that the influence of magnetization tolerances on cogging torque is more significant as on back-EMF. This means, that on the one hand the machine's behavior is strongly influenced in general. But on the other hand, as a cogging torque test is excluded for an end-of-line concept, it implies high functional requirement of the measurement devices to detect faults by use of back-EMF analysis. This shows the importance of an influence analysis such as presented in this study. It is required to study the impact of tolerances to be able to separate it towards measurement inaccuracy.

VI. Conclusion

In this work, the influence of non-ideal manufactured rotor components of a PMSM on its back-EMF and current characteristic is studied. It has been shown that electrical quantities are applicable to realize tolerance diagnosis. Especially the stator current approves to be a promising approach due to its time- and cost-saving setup. The new harmonic orders caused by rotor faults are derived within a theoretical analysis and confirmed by the simulation results.

An end-of-line check could be realized in such a way that all machines presenting a certain level in these specific characteristics are rejected. With the presented methods, the range of these distinguishing characteristics can be evaluated to detect the corresponding levels for rejection. At this, measurement accuracy should be taken into account.

Comparing the different rotor tolerances, all present the same characteristics but with different amounts depending on the fault's intensity and arrangement. As a feedback for manufacturing, a differentiation of various tolerances would be gainful but can not be achieved with the presented analysis. However, the focus of the end-of-line check is to verify the machines' quality which can be realized by the suggested approach. The results of this study evince to be valueable for application of an accurate quality control for PMSMs finally improving its reliability.

References

[1] S. Nandi, H.A. Toliyat, and X. Li, "Condition Monitoring and Fault Diagnosis of Electrical Motors - A Review," IEEE Transactions on Energy Conversion, vol. 20, no. 4, pp. 710-729, December 2005.

[2] L. Gasparin, A. Cernigoj, S. Markic, and R. Fiser, "Additional Cogging Torque Components in Permanent-Magnet Motors Due to Manufacturing Imperfections," IEEE Transactions on Magnetics, vol. 45, no. 3, pp. 1210-1213, March 2009.

[3] P.J. Tavner, "Review of condition monitoring of rotating electrical machines," IET Electric Power Applications, vol. 2, no. 4, pp. 215247, 2008.

[4] W. le Roux, R. G. Harley, and T. G. Habetler, "Detecting Rotor Faults in Low Power Permanent Magnet Synchronous Machines," IEEE Transactions on Power Electronics, vol. 22, no. 1, pp. 322-328, January 2007.

[5] D. Casadei, F. Filippetti, C. Rossi, A. Stefani, and D.J. Ewins, "Magnets faults characterization for Permanent Magnet Synchronous Motors," IEEE International Symposium on Diagnostics for Electric Machines, Power Electronics and Drives, pp. 1-6, 2009.

[6] A. Flach, F. Drager, M. Ayeb, and L. Brabetz, "A New Approach to Diagnostics for Permanent-Magnet Motors in Automotive Powertrain Systems," IEEE International Symposium on Diagnostics for Electrical Machines, Power Electronics and Drives, pp. 234-239, September 2011.

[7] G. Heins, T. Brown, and M. Thiele, "Statistical Analysis of the Effect of Magnet Placement on Cogging Torque in Fractional Pitch Permanent Magnet Motors ," IEEE Transactions on Magnetics, vol. 47, no. 8, pp. 2142-2148, August 2011.

[8] J.R. Cameron, W.T. Thomson, and A.B. Dow, "Vibration and current monitoring for detecting airgap eccentricity in large induction motors," IEE Proceedings B Electric Power Applications, vol. 133, no. 3, pp. 155 - 163, May 1986.

[9] B.M. Ebrahimi, J. Faiz, and M.J. Roshtkhari, "Static-, Dynamic- and Mixed-Eccentricity Fault Diagnoses in Permanent-Magnet Synchronous Motors," IEEE Transactions on Industrial Electronics, vol. 56, no. 11, pp. 4727-4739, November 2009.

[10] J. Urresty, J. Riba Ruiz, and L. Romeral, "A Back-emf Based Method to Detect Magnet Failures in PMSMs ," IEEE Transactions on Magnetics, July 2012.

[11] T. Herold, D. Franck, E. Lange, and K. Hameyer, "Extension of a D-Q Model of a Permanent Magnet Excited Synchronous Machine by Including Saturation, Cross-Coupling and Slotting Effects," International Electric Machines and Drives Conference (IEMDC), pp. 1379-1383, 2011.

[12] C. Schlensok, D. van Riesen, B. Schmülling, M. Schöning, and K. Hameyer, "Cogging Torque Analysis on Permanent Magnet Machines by Simulation and Measurement," tm - Technisches Messen, vol. 74, no. 7-8, pp. 393-401, August 2007.

[13] I. Coenen, M. van der Giet, and K. Hameyer, "Manufacturing Tolerances: Estimation and Prediction of Cogging Torque Influenced by Magnetization Faults," IEEE Transactions on Magnetics, vol. 48, no. 5, pp. 1932-1936, May 2012.

[14] I. Coenen, M. Herranz Gracia, and K. Hameyer, "Influence and evaluation of non-ideal manufacturing process on the cogging torque of a permanent magnet excited synchronous machine," COMPEL, vol. 30, no. 3, pp. 876-884, 2011.

[15] K. Kim, S. Lim, D. Koo, and J. Lee, "The Shape Design of Permanent Magnet for Permanent Magnet Synchronous Motor Considering Partial Demagnetization," IEEE Transactions on Magnetics, vol. 42, no. 10, October 2006.